

Tailored Torsion and Bending-Resistant Avian-Inspired Structures

Federica Buccino, Paolo Bruzzaniti, Sara Candidori, Serena Graziosi, and Laura Maria Vergani*

The escalating demand for torsion- and bending-resistant structures paired with the need for more efficient use of materials and geometries, have led to novel bio-inspired ingenious solutions. However, lessons from Nature could be as inspiring as they are puzzling: plants and animals offer an enormous range of promising but hierarchically complex configurations. Avian bones are prominent candidates for addressing the torsional and bending issue. They present a unique intertwining of simple components: helicoidal ridges and crisscrossing struts, able to bear flexural and twisting actions of winds. Here, it is set how to harmonically move from the natural to the engineering level to formalize and analyze the biological phenomena under controlled design conditions. The effect of ridges and struts is isolated and combined toward tailored torsion and bending-resistant arrangements. Then the biological level is revisited to extrapolate the avian allometric design approach and is translated into multiscale lightweight structures at the engineering level. This study exploits the complexity of Nature and the scalability that characterizes the evolutionary design of bird bones through the design and fabrication versatility allowed by additive manufacturing technologies. This paves the way for exploring the transferability of the proposed solution at multiple engineering scales.

structures are characterized by articulated geometries,^[2–4] high weight,^[5] intricate design,^[6] and high manufacturing costs.^[7] Additionally, the torsional issue is a multifaceted problem that traditional design approaches and materials cannot satisfactorily meet in terms of cost–benefit ratio.^[8,9]

On the contrary, Nature is not limited by geometric complexity and has already actively responded to the torsional issue by designing helicoidal patterns, which are versatile building blocks implied to improve the mechanical performance of load-bearing biological materials. These arrangements can deform in a spring-like manner, enhancing the absorption of deformation energy. The idea of combining soft bio-inspired helical fibers in a stiff matrix is a fascinating solution.^[10] Indeed, assessing the contribution of the overall fiber architecture and its design variables (e.g., helix pitch, rotary angles, number of helix reinforcements) on the interlaminar shear resistance can open stimulating scenarios for their implementation


as an engineering solution. In this context, practical attempts are already made to exploit such a helix-based arrangement to fabricate new composite materials.^[11] A relevant approach, in multi-objective optimization, to enhance both stiffness and failure strain is to mimic the wood structure and its multilayer helicoidal arrangement.^[12,13] The primary outcome that emerges is, in fact, the capability of the helicoidal design to improve torsion resistance. Even by simply modifying the fiber direction, it is possible to tune the local mechanical behavior of bio-inspired structures without altering the material chemistry.^[12] However, while presenting high versatility in the design phase, previous bio-inspired structures suffer from realization complexity due to the elaborate helicoidal patterns. Such a level of intricacy limits the technical feasibility of the proposed solutions and their transferring and scalability to real-world engineering problems.^[14] Hence, while the investigation of the effectiveness of biological systems in facing torsional loads should be fostered, it is also essential to reflect on how to properly transfer such solutions outside the natural world by, for instance, exploiting the potential of currently available manufacturing technologies.

Among all biological structures, bone-inspired ones are deepened since bone is a performant natural load-bearing material,

1. Introduction

The intrinsic complexity of torsional load, its 3D nature, its interplay with other stresses (especially bending), and its disruptive impact in several engineering sectors make torsional failure prevention an ambitious target. However, commonly designed torsion-resistant structures suffer from several limitations despite the wide range of applicative fields, such as civil, mechanical, marine, and biomedical engineering,^[1] where torsional failures still represent widespread critical issues. Current torsion-resistant

F. Buccino, P. Bruzzaniti, S. Candidori, S. Graziosi, L. M. Vergani
Department of Mechanical Engineering (DMEC)
Politecnico di Milano
Via La Masa 1, 20156 Milano, Italy
E-mail: laura.vergani@polimi.it

 The ORCID identification number(s) for the author(s) of this article can be found under <https://doi.org/10.1002/adem.202200568>.

© 2022 The Authors. Advanced Engineering Materials published by Wiley-VCH GmbH. This is an open access article under the terms of the Creative Commons Attribution License, which permits use, distribution and reproduction in any medium, provided the original work is properly cited.

DOI: 10.1002/adem.202200568

extremely tough but lightweight, presenting an efficient design characterized by a simple constituting element arrangement.^[15,16] Despite the favorable behavior of bone-inspired geometries^[17–21] under compressive loads, no prior consideration has been performed under torsional load since human bones rarely experience it. There are few animals whose bones are optimized to sustain torsional and bending loads; this is the case with birds. During the flight, a wing produces a lift equal to the downward impulse of the surrounding air, where the wing carrying capacity depends on its size, airspeed, air density, and angle of attack. To have a stable flight, lift must equal weight.^[22] This lift force F is equally divided between the two wings. Moreover, drag also imposes moments on the wings, but these drag-induced moments are negligible if compared to the weight-induced ones and could be ignored.^[23] As a result of these loading conditions, the ulna disposes itself roughly perpendicular to the humerus. Because of this large angle between the two bones, bending moments applied by the lift force to the radio-ulna are transmitted to the humerus primarily as twisting moments and vice versa.^[24] For the sake of simplicity, the wing can be considered a series of thin airfoils; the torsion arm is the distance between the center of lift of a given air foil and the neutral axis of torsion of the bone. The bending arm is the distance between the center of lift and an axis at 90° with respect to the torsion axis. The most stressed zone of the entire wing apparatus is located approximately one-third from the proximal end of the humerus.^[24,25] Regarding physical properties, bird bones are lightweight since they have a hollow cross-section; this is the result of a long evolution and adaptation process aimed at reducing the metabolic cost of flight. Bone density data show that birds have the densest bone ($\approx 2.15 \text{ g cm}^{-3}$) compared with other animal classes.^[26] Many bird bones are composed primarily of cortical bone, which is less porous than cancellous bone and has higher mineral content. Indeed, on average, bird skeletons are stronger and stiffer relative to their weight than are the skeletons of mammals.^[26] In other words, this implies that bird skeletons have higher strength-to-weight and stiffness-to-weight ratios.^[24,26] By looking at the microstructure, the humerus and ulna have a higher degree of laminarity and higher incidences of oblique collagen fibers than the radius, the carpometacarpus, and the tibiotarsus, which are bones not directly involved in the flight. This arrangement of fibers has been hypothesized to be an additional feature to increase torsion resistance.^[8,27]

Anyway, the hollow cross-section makes avian bones less resistant in absolute values than cortical bones of mammals. To offset this drawback and increase mechanical resistance, Nature has provided bird bones with two peculiar features that are a core source of inspiration: ridges and struts. Ridges are protrusions of bone that lie flat against the interior walls. In avian bone, they generally develop at an angle between 25° and 60° to the horizontal axis of the bone to increase the resistance of the structure to the large tensile stresses that develop in these directions when subjected to torsional loadings. Struts, instead, are isolated rods that stretch across the interior of the pneumatic bone. They are mainly found on the ventral side of wing bones of flying birds, appearing to be at locations with a higher risk of local buckling due to combined bending and torsion loading. Two types of reinforcing struts can be distinguished; the first one supports the hollow center of the bone against the vocalization and the second

one (an array of crisscrossing struts, resembling a truss) appears at places “in need”, supporting the bone against the extensive torsional stresses during flight.^[24,28,29]

All the mentioned reasons make avian bone a prominent candidate for the multiobjective design of torsion and bending resistant structures. Preliminary works test and explore the effects of struts alone, proving that they effectively increase the resistance to buckling while not improving the torsional stiffness.^[28,29] Nevertheless, no study explores the combined arrangement of struts and ridges as an ideal recipe to optimize and tailor bending and torsion resistance. Understanding the intimate cross-links between design criteria and functional requirements of avian bones can help tackle the weaknesses that limit a multiobjective design.

This work focuses on the design of an avian-bone-inspired architecture, containing the distinguishing features that make it effective for torsional and flexural resistance. To increase the chances of applicability of the proposed concept to real-world engineering problems, the biological solution has been formalized through engineering parameters that include its fabricability with state-of-the-art 3D printing machines. Such a formalization process is not straightforward because there are remarkable differences between Nature's design process and the engineering one concerning the materials employed and the approach implemented. Indeed, Nature designs the organism, implying principles of self-assembly and providing control at all hierarchical levels.^[30–32] The transferring of a natural principle into an engineering context should be first performed by investigating the contribution of each natural feature to the overall design target, followed by an analysis of their biomechanical interplay. Each natural component should not be merely scaled in terms of dimensions but reinterpreted in light of the new boundary conditions. Besides, since Nature applies an evolutionary and multi-scale design approach, the mentioned process should explore and implement the scaling law that drives the transferring of the solution at multiple scales. Due to their large variability in size and exceptional flying ability under different loading conditions, bird bones appear the most prominent candidate for investigating scaling effects. The length of wing bones (humerus and ulna) scales more steeply with mass than the length of hindlimb bones (femur),^[33] meaning that longer airfoils are required to support a heavier load by the generated lift. Moreover, the diameter of the bone increases at a slower rate compared to its length. In other words, birds' bones become relatively thinner as they become longer. Additionally, larger birds have a higher aspect ratio (i.e., the ratio between the square of the wingspan and wing area) for the wings, despite the wing area varies isometrically.^[34] The aforementioned scaling behavior has a significant effect: stresses in humeri are scale-independent and constant. Moreover, to achieve this result, the ratio between the outer and inner diameter of the bone remains constant.^[23,35]

In the proposed avian-bone-inspired architecture, struts are schematized as “beams” while ridges as helices. For ridges-containing configurations, parameters like the position (inner or outer) of the helix angle, the spacing between helices, and the possibility of having a specular arrangement of such helices are studied. At the same time, in the case of struts-configurations beam-like struts and crisscrossing struts are investigated. Then, these features are combined in the same structure to evaluate the

optimal torsion and bending-resistant architecture. Eventually, the *scaling law*, which characterizes the multiscale and evolutionary design of avian bones, is applied to explore the transferability of the proposed solution at multiple engineering scales.

2. Results and Discussion

The formalization process we exploit for addressing the torsional and bending resistance issue follows a multilevel path (Figure 1). The starting point is the natural level, where the inspiration takes place, considering avian bones as prominent candidates for their unique intertwining of two simple components, i.e., helicoidal

ridges and crisscrossing struts (Figure 1A). A transitional level simplifies ridges as helicoidal-like arrangements and struts as beam-like components (Figure 1B). The engineering level (Figure 1C) deepens a wide range of geometrical parameters related to three main categories: ridges-only, struts-only, and combined structures. Computational simulations are conducted to quantify the expected improvements in torsional and bending resistance of the designed configurations, aiming to tune their mechanical response to the mentioned loading conditions. The re-connection to the biological world (Figure 1D) is reached through the avian bone scaling law: we demonstrate that engineering structures, whose diameter and length are progressively varied according to the mentioned law, exhibit scale-independent stress trends.

At the engineering level (Figure 1C), first, we identify a baseline structure (B_s) as a reference, characterized by neither helices nor internal beams. We then design and computationally analyze struts-only, ridges-only, and combined ridges-struts configurations (Figure 1C). These multiple configurations allow us to assess the structural contribution of each natural feature that composes the biological system of interest. All the presented structures are sketched with constant mass with respect to B_s . Concerning struts-only configurations (S), we deepen two kinds of arrangements. In the first group of configurations (ten in total), reinforcement structures do not intersect. Specifically, three configurations (i.e., S_{1a} , S_{2a} , and S_{3a} in Figure 1C, bottom-left) have struts distributed along a single direction identified by the “ a ” axis (Figure 1B). Six configurations present struts distributed along two perpendicular directions (i.e., S_{1a-1b} , S_{2a-1b} , S_{3a-1b} , S_{2a-2b} , S_{3a-2b} , and S_{3a-3b} in Figure 1C, bottom-left), identified by the “ a ” and “ b ” axes (Figure 1B). The last architecture shows struts mutually inclined at 45° (i.e., S_{45° in Figure 1C, bottom-left). In this first group of configurations, nonparallel beams are located on different planes, spanning the cylinder length at a constant pitch (Figure 1C). On the contrary, the second group of struts-only configurations has struts that intersect each other (the label “ X ” is used in Figure 1C to identify them). They have two series of crossing struts repeated along the cylinder. The inclination angle α is equal to 30° , 45° , and 60° , respectively (i.e., S_{X30° , S_{X45° , and S_{X60° in Figure 1C, bottom-left). We tested both types of configurations to evaluate the contribution of the beam as a single element and the beam as part of a network because both configurations can occur in avian bones.^[28]

For ridges-only structures (R), the helix number is kept constant equal to four, as a typical arrangement in avian bones.^[29] Parameters such as the position (R_e external, R_i internal, Figure 1C, bottom-right), helix angle β (30° , 45° , and 60° , Figure 1C, bottom-right) and spacing angle between helices θ (20° , 45° , 90° , Figure 1C, bottom-right) are studied. Three additional configurations containing specular (R_x , Figure 1C, bottom-right) ridges are designed too, exploiting the concept of symmetry, which is a typical natural pattern and a practical engineering strategy adopted for simplification issues.^[36]

The conclusive step in addressing avian bones as a solution for improving torsional and bending stiffness is to combine struts (S) and ridges (R) in a unique structure containing both these features. Four different configurations are analyzed: three $S_{X\alpha}R_{e45^\circ,90^\circ}$, with α equal to 30° , 45° , 90° (Figure 1C, top) and

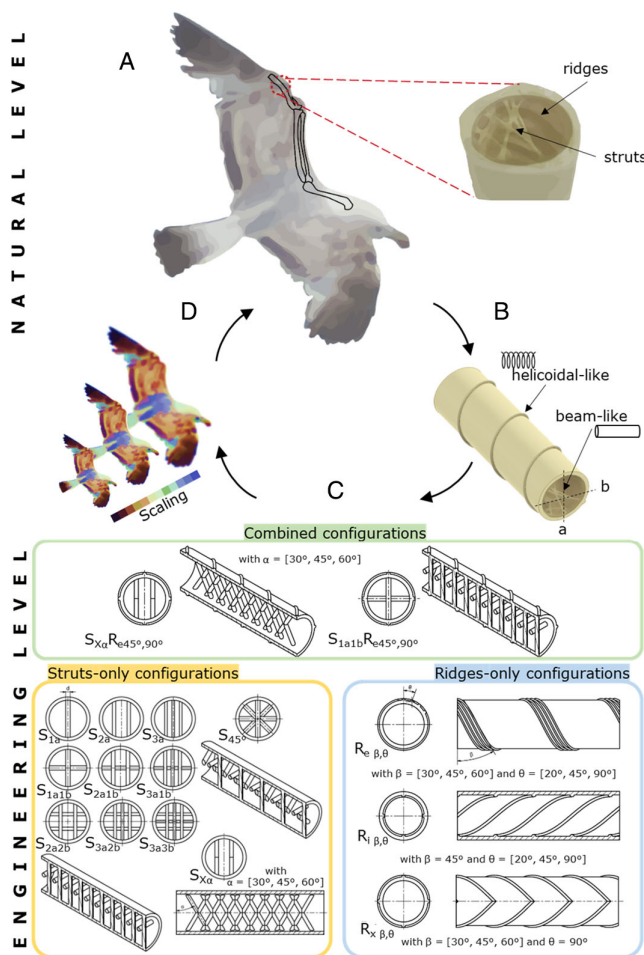


Figure 1. Overview of the implemented bio-inspired approach and of the multilayer model design: A) the inspiration derives from the natural level. Bird bones are selected for their lightweight arrangement with two simple intertwining elements, i.e., ridges and struts. B) moving from the biological to the engineering level, a transitional level is required in which helicoidal and beam-like components are isolated as prominent candidates for combined torsional and bending resistant structures. C) the whole engineering level is the result of a conceptualization in which three configurations are explored: ridges-only (light-blue box), struts-only (yellow box), and combined structures (green box). For each category, multiple design parameters are explored. D) the re-connection from the engineering to the natural level is ensured by the scaling approach, stating the scale-independency of the stresses.

intersecting struts (label “X”), and one $S_{1a1b}R_{e45^\circ,90^\circ}$ (Figure 1C, top) with nonintersecting struts.

Considering the expansion of different configurations to be investigated, we reduced the parameter space through computational simulations under torsional and bending loads for ridges and struts-only configurations, respectively (Figure 2). Combined structures are tested under torsional and flexural loads (Figure 3).

First, the contribution to the increase in the flexural stiffness is discussed in struts-only configurations in comparison to the reference structure B_s . The alignment of struts with respect to the load direction, as in the S_{1a} arrangement (Figure 1C, bottom-left), is beneficial for enhancing the bending stiffness (+65% with respect to B_s , Figure 2A). The relative position of the three-point-bending supports is kept constant in all structures. The increasing number of struts passing from one configuration to another does not appear to affect the bending stiffness since they get comparable outputs (Figure 2A), with the S_{1a-1b} being the second stiffest (+44%) and the S_{3a-2b} being the third one (+40%). Configurations having crisscrossing struts (i.e., S_{X30° , S_{X45° , S_{X60° , Figure 1) are the least stiff among all the reinforced structures (together with the S_{45°), also showing the lowest increase (<20%) in the strain energy absorption with respect to B_s (Figure 2C) and the lowest increase in the maximum von Mises stress (Figure 2E). The S_{X60° arrangement exhibits a reduction in the strain energy absorption as compared to the baseline, with a significant additional increase (>60%) in the maximum von Mises stress (Figure 2C–E).

Configurations having outer ridges (R_e) have higher stiffness and strain energy absorption than structures having internal ones (R_i), as shown in Figure 2B,D, respectively. This behavior can be understood by noticing that, in the case of external ridges, most of the material distribution is in the periphery of the torsional axis, i.e., the inertia is increased. Concerning the helix angle β , configurations with ridges at 45° are optimal in increasing the torsional stiffness and strain energy absorption, in agreement with previous works exploring the sole effect of helicoidal arrangements.^[37,38] Indeed, under pure torsion, the stress state is defined by the principal stresses $\sigma_I = \tau$ and $\sigma_{III} = -\tau$, which are placed at $\pm 45^\circ$ with respect to the cylinder axis. Therefore, increasing the inertia along these directions will enhance the mechanical response. Moreover, in the perspective of bio-inspiration, this inclination angle is the most commonly found in birds’ bones.^[24] Another investigated parameter is the spacing between helices (at a fixed helix angle); in this case, configurations with θ corresponding to 90° (Figure 1C, bottom-right) are the stiffest because reinforcements are homogeneously distributed along the whole structure. The torsional stiffness in structures with specular ridges (R_s) is comparable in configurations characterized by the same θ and β values. The main difference is in the maximum von Mises stress value, which increases from a minimum of 15% in the case of $R_{X30^\circ,90^\circ}$ (Figure 1C, 2F) up to a maximum of 35% in the case of $R_{X45^\circ,90^\circ}$ compared to structure B_s (Figure 1C, 2F). Predictably, the most stressed zone is the one where there is an abrupt change in the helix angle, which passes from $-\theta$ to $+\theta$. Summing up, the stiffest configuration among the ridges-only ones is the $R_{e45^\circ,90^\circ}$ (Figure 1C), which shows an increased torsional stiffness of 5.4% with respect to structure B_s (Figure 2B).

For the configurations characterized by the combined effect of ridges and struts (i.e., $S_{X\alpha}R_{e45^\circ,90^\circ}$, and $S_{1a1b}R_{e45^\circ,90^\circ}$, Figure 1C, top) as commonly visible in avian bones, numerical analyses confirm that for non-crisscrossing struts, the torsional stiffness is practically the same as a ridges-only structure (101 N m rad^{-1} vs 100 N m rad^{-1} , which corresponds to an increase of around 5% with respect to the reference structure, Figure 3A). Looking at the crisscrossing struts configurations, we see that they effectively increase the torsional stiffness by a value between 6.9% and 7.3% compared to the B_s configuration (Figure 3A). The same increasing trend is visible in the strain energy absorption (Figure 3B). Once again, 45° is the optimal angle even for the strut inclination. A slight increase (2.5–4%) of the bending stiffness with respect to the corresponding struts-only structures can be observed in all structures. This increment can be interestingly attributed to the presence of ridges. The torsional von Mises maximum stresses confirm this trend (Figure 3C).

The formalization and parameterization of the building blocks of the analyzed structures allow us to exploit extrusion-based 3D printing techniques with a twofold purpose. On the one hand, printing and subsequent experimental testing allow for validating the wide dataset of numerical simulations. On the other hand, the feasibility of the printing process plays a core role in the transition from engineering back to the natural level (Figure 1D). For these purposes, we use an FFF (Fused Filament Fabrication) 3D printer to fabricate our avian bone-inspired designs. The values of the geometric features of the samples are selected to guarantee the printability of the analyzed configurations (see Supporting Information). The 3D-printed samples allow to characterize the configuration behavior, test their technical feasibility, and validate the numerical models.

The tested specimens are shown in Figure 4A,B together with the torque–rotation (torsional tests) and load–displacement (bending tests) curves. The torsional curves present an initial plateau, possibly due to the testing machine compliance. After this plateau, the slope of the linear range is practically equal to the numerical results (the maximum difference is in the order of 1%). Moreover, the minimal extent of the nonlinear region suggests that the use of a linear-elastic model to describe material behavior is correct. The $R_{e45^\circ,90^\circ}$ (Figure 4A, middle) and $S_{1a1b}R_{e45^\circ,90^\circ}$ (Figure 4A, bottom) configurations present a higher torsional stiffness compared to the B_s structure (Figure 4A, top), confirming that the reinforcements are effective in increasing the mechanical behavior.

The stiffness values obtained through the experimental results are not the actual values of the designed structures because they are affected by the specimen geometry. The introduction of a square geometry at the ends is an essential requirement to allow the testing machine to grip the sample properly and inevitably alter the stress distributions. According to the numerical analyses, the magnitude of this reduction is about 12–13%. Since experimental results confirm these values, the stiffness values of the structures obtained by numerical analyses can be considered reliable. Regarding comparing different designs, the ridges increase the torsional stiffness by about 6% compared to structure B_s , both having the same mass. $S_{1a1b}R_{e45^\circ,90^\circ}$ shows an identical stiffness of $R_{e45^\circ,90^\circ}$ but the presence of struts slightly extends the nonlinear plateau before the failure (Figure 4).

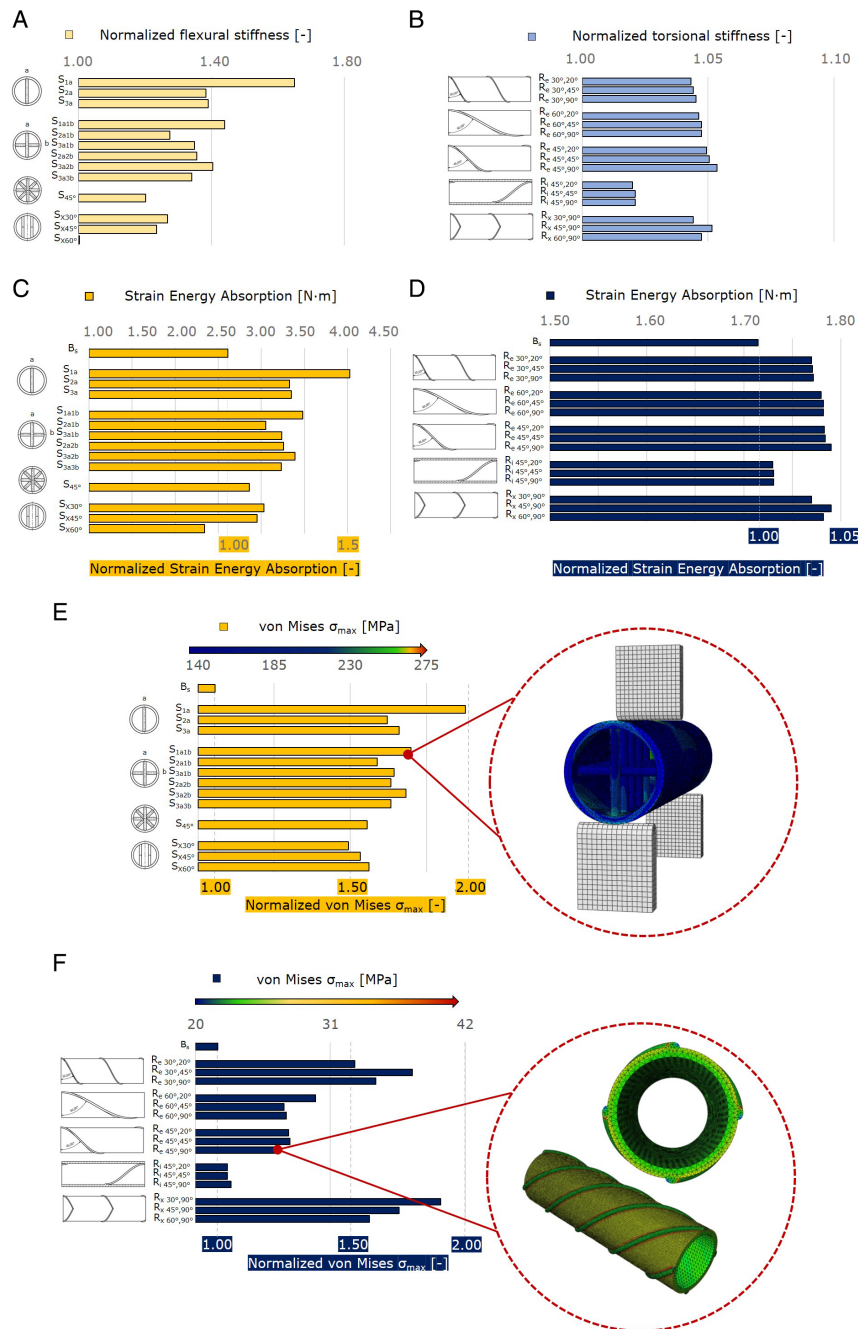


Figure 2. A) Normalized flexural stiffness with respect to the reference structure B_s of struts-only configurations. The flexural stiffness of the reference structure B_s is equal to 228 N mm^{-1} . B) Normalized torsional stiffness with respect to the reference structure B_s of ridges-only configurations. The torsional stiffness of the reference structure B_s is equal to 95 N m rad^{-1} . C) Strain energy absorption (absolute and normalized values with respect to B_s) of the struts-only configurations. D) Strain energy absorption (absolute and normalized values with respect to B_s) of the ridges-only configurations. E) von Mises maximum stress (absolute values and normalized values with respect to B_s) of struts-only configurations. F) von Mises maximum stress (absolute values and normalized values with respect to B_s) of ridges-only configurations. All the stiffness, strain energy absorption, and von Mises stress values are obtained from numerical simulations. The torsional stiffness is computed as the line slope interpolating the reaction moment vs-imposed rotation graph while bending stiffness is obtained as the line slope interpolating the reaction force vs crosshead displacement graph data. Strain energy absorption is calculated as the area under the reaction moment vs imposed rotation graph in the torsional case and reaction force vs crosshead displacement graph in the flexural case. Details of the finite element method (FEM) analysis are reported for the most prominent configurations.

Concerning the bending tests performed on B_s (Figure 4B, top), S_{3a2b} (Figure 4B, middle), and $S_{1a1b}R_{e45^\circ,90^\circ}$ (Figure 4B, bottom) structures, it clearly appears that the experimental analyses

validate the numerical models. S_{3a2b} and $S_{1a1b}R_{e45^\circ,90^\circ}$ configurations present a higher stiffness but a much lower maximum deflection (1.5 mm vs 3.2 mm) with respect to B_s . The printing

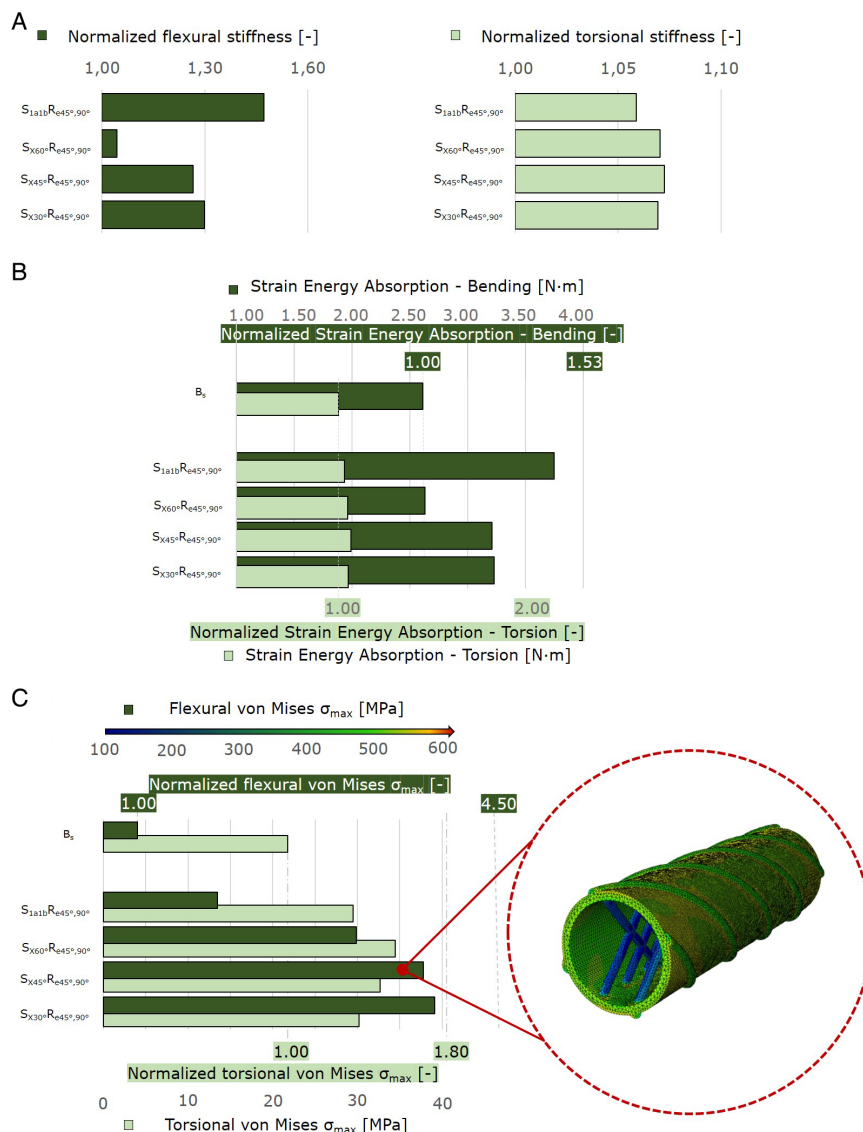


Figure 3. Numerical results of torsion and three-point-bending simulations on ridges + struts structures (i.e., combined configurations in Figure 1). A) Normalized flexural (left) and torsional (right) stiffness with respect to the reference structure B_s . The flexural and torsional stiffnesses of the reference structure B_s are equal to 228 N mm^{-1} and 95 N m rad^{-1} , respectively. B) Strain energy absorption (absolute and normalized values with respect to B_s) of the ridges + struts structures configurations. C) Flexural and torsional von Mises maximum value (absolute value and normalized with respect to B_s) detected in ridges + struts arrangements. A detail of the FEM analysis is provided for $S_{X45^\circ}R_{e45^\circ,90^\circ}$.

direction and the layer deposition affect the experimental results and in particular the failure mode, as highlighted in the dashed circles. Indeed, the printing direction follows a circular path in the B_s layer deposition, differently from what happens in the other arrangements. The main consequence is that the adhesion between layers varies inside the same structure (S_{3a-2b} and $S_{1a1b}R_{e45^\circ,90^\circ}$), while is constant for the baseline. This has a specific effect on the failure modes: indeed, in experimental three-point-bending tests, failure does not occur in the middle of the specimen, as expected, but is located at the region where the layer adhesion is insufficient to withstand the resulting stresses. On the contrary, this is not detectable in B_s , where layer deposition is homogeneous in the overall structure.

As the last step of the study, we used the $S_{1a1b}R_{e45^\circ,90^\circ}$ configuration resulted in the most notable increase in torsional and flexural stiffness to implement the scaling law^[23,34,35] through the allometric Equation $D = 0.32 L^{0.8}$, in which D is the internal diameter of the structure and L its length (Figure 4C). We scaled the $S_{1a1b}R_{e45^\circ,90^\circ}$ length, and diameter following this rule; internal struts and external ridges are scaled accordingly. We apply a fixed support on one end and a torsion + external distributed load on the scaled configurations, mimicking the wind effect. The computational analyses affirm that the resulting stresses are not scale-dependent for this configuration, and they remain constant when increasing the length scales. As in natural arrangements, engineering structures following the scaling

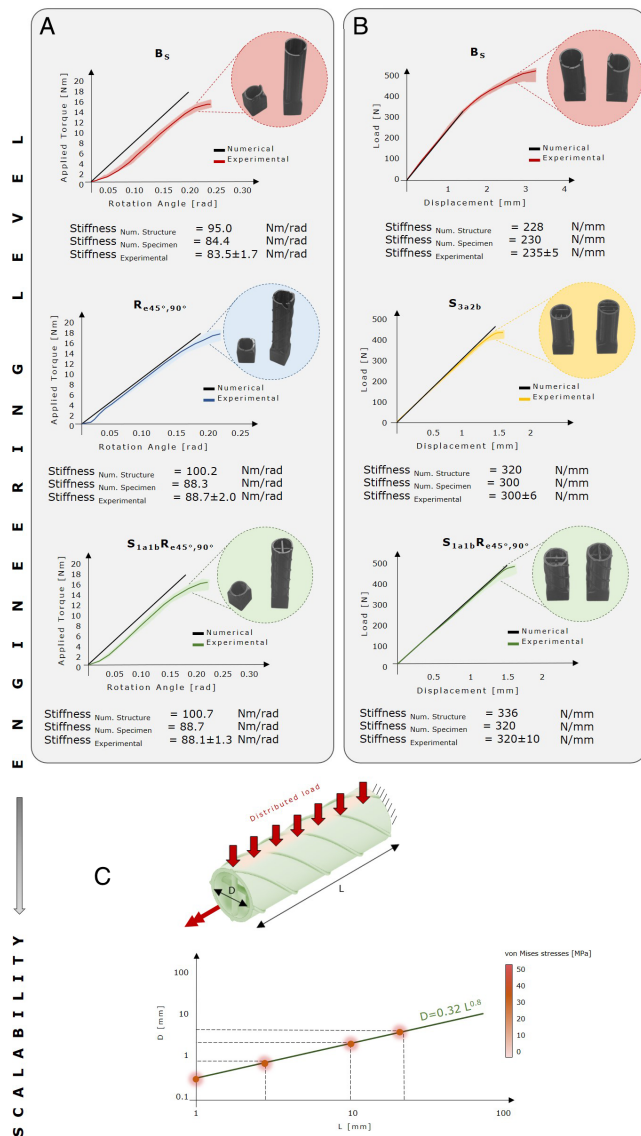


Figure 4. Validation of numerical models, technical feasibility analysis, and exploitation of the allometric rule. A) Experimental torsional tests compared to numerical results. A, top) The B_s structure computational model (black line) is validated through experimental tests under torsion (red line) performed on the 3D-printed sample. Experimental tests are repeated for three identical B_s , and the test scatter is reported with a pinkish halo. The same approach is adopted for the most prominent configuration in terms of torsional resistance (A, middle, $R_{e45^\circ, 90^\circ}$) and for the combined $S_{1a1bR_{e45^\circ, 90^\circ}}$ arrangement (A, bottom). The failure mode of each structure is highlighted in a dashed circle. B) Experimental three-point-bending tests (three for each specimen category) compared to numerical results. In the case of B_s (B, top), S_{3a2b} (B, middle) and $S_{1a1bR_{e45^\circ, 90^\circ}}$ arrangements (B, bottom). C) These verifications allow for numerically exploiting the scalability concept. Four designs for the $S_{1a1bR_{e45^\circ, 90^\circ}}$ category are considered (red circles), and their length and internal diameter are varied following the allometric law. One side of the configurations exhibits a fixed support; a distributed and a torsional load are applied to mimic the effect of the wind on avian wing bones. The graph shows the von Mises stresses detected in the four allometric configurations, demonstrating no significant variations when the length and diameter are tuned as the allometric law.

law display efficient stress distribution across length scales, keeping a constant safety factor. In the natural world, this is a synonym of optimum identification: indeed, through an allometric equation, Nature succeeds in avoiding the reduction of the safety factor, practically resulting in all avian bones, independently of their dimensions, being able to sustain the torsional and flexural effect of wind on their wings. The same concept remains unaltered when this allometric approach is transferred into engineering configurations.

3. Conclusions

Despite the increasing impact of failures due to torsional loads and the related burden on several engineering fields, standard-designed structures are still far from representing a suitable strategy to overcome that issue. In addition, even though Nature often deals with torsional loads, bio-inspired solutions are frequently either on a preliminary stage or too intricate to be applied on a wide scale.

In this work, we exploit avian bone structures as an intelligent solution where simple elements, i.e., ridges and struts, are appropriately combined to enhance torsional and bending resistance. Besides, we also design the bio-inspired architecture to guarantee its technical feasibility and its potential in terms of scalability. We take advantage of the synergy between ridges and struts to design and realize novel 3D-printed avian bone-inspired structures optimized for torsional and bending resistance. Parameters such as the pitch angle of the ridges and the number of struts are varied to obtain several configurations of interest. In contrast, the mass of ridges and struts is kept constant to have a meaningful comparison between different arrangements.

According to finite element analyses, outer ridges are more effective in increasing the torsional stiffness and strain energy absorption with respect to inner ridges because the inertia is enhanced. Regarding the helix angle, 45° has the optimal behavior, as expected, and the ideal spacing between helices is 90° . Concerning bending, the stiffest structure is characterized by struts parallel to the load direction, with an increase of stiffness of 65% compared to a nonreinforced architecture. By combining ridges and struts, we demonstrate that beam-like struts play a limited role in increasing torsional stiffness and strain energy absorption, while crisscrossing struts (45° inclination) can increase torsional, bending stiffness, and strain energy absorption compared to struts-only arrangements.

The testing of several configurations allowed tuning struts and ridges parameters toward the desired load resistance. The 3D printing and consequent mechanical testing of the most prominent geometries validate the numerical models and enhance the sketched structure core potentialities. It is worth mentioning the easiness of realization because the complexity of struts disposition is intentionally kept at the minimum and the versatility of the structures for both torsional and bending load resistance. Eventual issues are linked to the layer adhesion in the printing process that has an effect on the failure modes of the tested configurations. Additionally, the coherence of our results with the allometric rule represents a prominent perspective for moving from sample-level analysis to multiscale applicative solutions. Indeed, these results have a relevant implication with respect

to the study's intent to exploit the potential of transferring biological avian-bone architectures into engineering solutions at multiple scales. Currently, the originality of the present work resides in the structural design of novel torsion and bending-resistant structures; however, given the avian inspiration, it would be challenging to combine a structure-based analysis with a material-based one. Indeed, the present study could pave the way for a suitable tuning of the mechanical properties as it happens in bones, that adapt dense and porous regions in accordance to the mechanical stimuli.

Moving to technical feasibility analysis, an extrusion-based desktop 3D printing machine was chosen for its effectiveness and simplicity. Therefore, its wide diffusion demonstrates its potential in the case of small-medium scale structures. It also represents, at a smaller scale, what is now happening on bigger scales in the field of architecture and construction engineering. In such fields, the extrusion process of concrete^[39–41] plays a significant role in demonstrating the potential of additive manufacturing (AM) technologies in satisfying the need of these sectors for sustainable and functional structures.^[39,41] Besides, advancements in the manufacturing process are combined with effective form-finding strategies that allow reducing the amount of material used for construction without altering the structural performance of the architecture.^[40] Among the available form-finding methods, biomimicry is an already well-known strategy in construction to design organic, efficient, and multifunctional structures.^[42] This consciousness further strengthens this study's intent concerning the possibility of exploiting the effectiveness of natural solutions at multiple scales. In addition, the architecture and construction fields are not the only ones working at bigger scales with extrusion-based processes. The naval industry also shows a relevant interest in this manufacturing technology.^[43] Therefore, lightweight and bio-inspired concepts could lead to sustainable and valuable solutions in multiple engineering fields. The wide diffusion, the multiscale capabilities, and the fertile research and industrial contexts that characterize AM technologies could thus be exploited to favor the implementability and the scalability of the proposed torsion and bending-resistant avian-inspired architectures. As demonstrated in this study, to reach this target, the proper transferring of the biological phenomenon to the real-world engineering context is essential. Such transformation should also include the technical limits implied by the manufacturing technology at disposal. The outcomes of this work can thus pave the way for challenging applications, for example, in the biomedical and construction fields, where the scaling factor is a crucial aspect that our avian-inspired structures could tackle. Indeed, considering small- and medium-size geometries, the pylon of transtibial prostheses could, for example, represent a fascinating implementation of our design. The pylon should combine lightness and stiffness, and according to ISO 10328,^[44] it must also overcome a static torsion test. Moving to large scales, a stimulating application of our avian-inspired structures could be the design of torsional dampers in earthquake-resistant buildings. Earthquake-induced torsion in buildings can be due to: a) nonsymmetric arrangement of the load resisting elements or nonsymmetric distribution of masses, b) torsional motion in the ground caused by seismic wave passage and by ground motion incoherency.^[5]

The promising results obtained from the printing process and the scaling analysis demonstrate that our bio-inspired configurations represent a suitable candidate even for wide-scale concepts because they were conceived as a combination of simple building blocks and by considering state-of-the-art manufacturing capability, as a demonstration of their technical feasibility.

4. Experimental Section

Sample Design: Model dimensions were defined considering printer resolution and the size of the characteristic features (i.e., struts and beams) with respect to the cylinder. Each strut or ridge-reinforced structure had a length of 67 mm, an external diameter of 20 mm, and a wall thickness of 1.5 mm. Ridge diameter ranged from 1.3 to 1.65 mm. Strut diameter is comprised between 1.2 mm (in S_{3a} and S_{3a-3b} configurations) and 2 mm (in S_{1a} , S_{45° , and S_{1a-1b} configurations).

Finite Element Simulations: The torsional and bending behavior of the structures were simulated with finite element analysis (Abaqus CAE, 2017). The torsional test was simulated for ridges-only structures by imposing a fixed support at one end; on the opposite side, a reference point was kinematically coupled with the surface. The imposed rotation was of 0.1 rad in such a way as to remain in the linearity assumption. From these analyses, stress distributions and reaction moments were obtained. Bending analyses, instead, were performed simulating the three-point bending test in the linearity field. The bending span was 65 mm, and the imposed crosshead displacement was 1.5 mm. Reference points were assigned to the contact regions between the structure and the loads. The friction coefficient was 0.2, which is a typical value for plastic material in contact with steel in clean and dry conditions. Additionally, the sliding of the specimen was prevented. From these analyses, stress distributions and reaction forces were obtained. A tetrahedral element (C3D10) with a free technique was chosen for the mesh. The optimal mesh size was selected by performing a sensitivity analysis on $R_{e45^\circ,90^\circ}$ and S_{1a} configurations (Supporting information). Element dimension equals 0.5 mm on the reinforcements (struts and ridges) and 1 mm elsewhere provided satisfactory convergence.

D Printing: Due to their morphological features, structures can be obtained only by exploiting an additive manufacturing process. In our case, a fused filament fabrication (FFF) 3D-printer (Ultimaker S5) was employed. This technique used material extrusion to print items, where a feedstock material was pushed through an extruder. The versatility of this machine was high, both in terms of printable geometries and exploitable materials. Polylactic acid (PLA), a thermoplastic polymer combining high tensile strength and surface quality, was chosen for printing high-resolution samples. PLA properties are: $E = 2346$ MPa and $\nu = 0.39$, as reported by the manufacturer.^[45] Printing parameters were tuned to balance resolution, layer adhesion and material consumption: Profile: fine = 0.1 mm; Layer height = 0.2 mm; Infill density = 100%; Brim width = 5 mm. Eventually, all the specimens were printed from the same spool to guarantee no eventual variation in terms of mechanical properties. To validate the numerical models, the following geometries were printed in triplicates to provide suitable statistical reliability: *Structure* B_s (nonreinforced structure) (six samples: three for torsional tests and three for bending tests), considered as a reference; $R_{e45^\circ,90^\circ}$ (three samples for torsional tests); S_{3a-2b} (three samples for bending tests); $S_{1a1b}R_{e45^\circ,90^\circ}$ (six samples: three for torsional tests and three for bending tests). Printed specimens presented a square geometry at each structure's extremities to prevent specimen sliding during tests. Furthermore, in the case of torsional tests, the specimen is inserted into ad hoc designed aluminum endcaps for machine gripping. The issue of having a change in sample cross-section affects stress distribution, generating stress concentrations in the transition region. This issue was minimized by setting the transition region to 5 mm.

Experimental Testing: 3D-printed specimens were tested in triplicates to have suitable statistical reliability. Displacement-controlled tensile tests were carried out to derive material characteristics at room temperature

using an MTS Alliance RT/100 universal tensile testing machine with a 100 kN load cell. A crosshead speed of 1 mm min⁻¹, corresponding to a strain rate of 4.6 × 10⁻⁴ s⁻¹, was adopted until failure. The displacement was measured through an extensometer MTS 635.25 F-05 with a gauge length of 25 mm. For torsional tests, the MTS809 servo-hydraulic triaxial machine was employed. The samples underwent an imposed angular displacement of 0.087 rad min⁻¹. For three-point bending, the MTS Synergie 200 electromechanical machine was exploited with a crosshead displacement of 1 mm min⁻¹.

Supporting Information

Supporting Information is available from the Wiley Online Library or from the author.

Acknowledgements

Open Access Funding provided by Politecnico di Milano within the CRUI-CARE Agreement.

Conflict of Interest

The authors declare no conflict of interest.

Data Availability Statement

The data that support the findings of this study are available in the supplementary material of this article.

Keywords

avian-inspired structures, bending resistance, scalability, torsion resistance, 3D printing

Received: April 20, 2022

Revised: July 19, 2022

Published online:

- [1] F. Buccino, G. Martinoia, L. M. Vergani, *Mater.* **2021**, *14*, 5368.
- [2] A. V. R. Leelavathi, *Int. J. Eng. Technol.* **2010**, *2*, 45.
- [3] W. Hao, Y. Liu, X. Huang, Y. Liu, J. Zhu, *Appl. Compos. Mater.* **2017**, *25*, 619.
- [4] W. Hao, Z. Huang, L. Zhang, G. Zhao, Y. Luo, *Compos. Struct.* **2019**, *229*, 111384.
- [5] J. M. Kelly, R. I. Skinner, A. J. Heine, *Bull. New Zeal. Soc. Earthq. Eng.* **1972**, *5*, 63.
- [6] M. Ismail, *Eng. Struct.* **2020**, *207*, 110092.
- [7] M. N. S. Hadi, L. C. Schmidt, *ACI Struct. J.* **2018**, *115*, 191.
- [8] E. De Margerie, S. Sanchez, J. Cubo, J. Castanet, *Anat. Rec. A Discov. Mol. Cell. Evol. Biol.* **2005**, *282*, 49.
- [9] M. Shama, *Torsion Shear Stress in Ships*, Springer, Germany **2010**, p. 1.
- [10] T. Tan, B. Ribbans, *Proc. R. Soc. A Math. Phys. Eng. Sci.* **2017**, *473*, 57.

- [11] M. M. Porter, L. Meraz, A. Calderon, H. Choi, A. Chouhan, L. Wang, M. A. Meyers, J. McKittrick, *Compos. Struct.* **2015**, *119*, 174.
- [12] L. Zorzetto, D. Ruffoni, *Adv. Funct. Mater.* **2019**, *29*, 1805888.
- [13] C. Zhao, L. Ren, Z. Song, L. Deng, Q. Liu, *J. Mech. Behav. Biomed. Mater.* **2019**, *89*, 132.
- [14] Y. Bouligand, *Tissue Cell* **1972**, *4*, 189.
- [15] F. Buccino, C. Colombo, L. M. Vergani, *Mater.* **2021**, *14*, 1240.
- [16] E. Goff, F. Buccino, C. Bregoli, J. P. McKinley, B. Aeppli, R. R. Recker, E. Shane, A. Cohen, G. Kuhn, R. Müller, *Bone* **2021**, *152*, 116094.
- [17] F. Libonati, G. X. Gu, Z. Qin, L. Vergani, M. J. Buehler, *Adv. Eng. Mater.* **2016**, *18*, 1354.
- [18] F. Libonati, C. Colombo, L. Vergani, *Fatigue Fract. Eng. Mater. Struct.* **2014**, *37*, 772.
- [19] F. Buccino, *IOP Conf. Ser. Mater. Sci. Eng.* **2021**, *1038*, 012039.
- [20] F. Buccino, C. Colombo, D. H. L. Duarte, L. Rinaudo, F. M. Ulivieri, L. M. Vergani, *Med. Biol. Eng. Comput.* **2021**, *59*, 2139.
- [21] F. Libonati, A. E. Vellwock, F. Ielmini, D. Abliz, G. Ziegmann, L. Vergani, *Sci. Rep.* **2019**, *9*, 1.
- [22] T. N. Sullivan, M. A. Meyers, *E. Arzt, Sci. Adv.* **2019**, *5*.
- [23] S. J. Kirkpatrick, *J. Exp. Biol.* **1994**, *190*, 195.
- [24] T. N. Sullivan, B. Wang, H. D. Espinosa, M. A. Meyers, *Mater. Today* **2017**, *20*, 377.
- [25] C. J. Pennycuick, *J. Exp. Biol.* **1967**, *46*, 219.
- [26] E. R. Dumont, *Proc. R. Soc. B Biol. Sci.* **2010**, *277*, 2193.
- [27] E. de Margerie, *J. Anat.* **2002**, *201*, 521.
- [28] E. Novitskaya, C. J. Ruestes, M. M. Porter, V. A. Lubarda, M. A. Meyers, J. McKittrick, *J. Mech. Behav. Biomed. Mater.* **2017**, *76*, 85.
- [29] E. Novitskaya, M. S. R. Vairo, J. Kiang, M. A. Meyers, J. McKittrick, *Adv. Bioceram. Biotechnol.* **2014**, *11*, 47.
- [30] P. Fratzl, *J. R. Soc. Interfaces* **2007**, *4*, 637.
- [31] U. G. K. Wegst, H. Bai, E. Saiz, A. P. Tomsia, R. O. Ritchie, *Nat. Mater.* **2015**, *14*, 23.
- [32] S. Weiner, H. D. Wagner, *Annu. Rev. Mater. Sci.* **1998**, *28*, 271.
- [33] M. Olmos, A. Casinis, J. Cubo, *Ann. Des. Sci. Nat. Zool. Biol. Anim.* **1996**, *17*, 39.
- [34] C. J. Pennycuick, in *Modelling The Flying Birds*, Elsevier, Amsterdam **2008**
- [35] G. J. M. Garcia, J. K. L. da Silva, *Phys. Life Rev.* **2006**, *3*, 188.
- [36] A. Modrea, V. M. Munteanu, I. Pruncu, *Proc. Manuf.* **2020**, *46*, 906.
- [37] F. Vollrath, R. Mi, D. U. Shah, *Curator Museum J.* **2018**, *61*, 95.
- [38] A. B. Kiladze, O. F. Chernova, *Data Br.* **2018**, *20*, 1700.
- [39] A. Jipa, B. Dillenburger, *3D Print. Addit. Manuf.* **2022**, *9*, 84.
- [40] J. Liu, V. Nguyen-Van, B. Panda, K. Fox, A. du Plessis, P. Tran, *3D Print. Addit. Manuf.* **2022**, *9*, 12.
- [41] A. Paolini, S. Kollmannsberger, E. Rank, *Addit. Manuf.* **2019**, *30*, 100894.
- [42] A. du Plessis, A. J. Babafemi, S. C. Paul, B. Panda, J. P. Tran, C. Broeckhoven, *Addit. Manuf.* **2021**, *38*, 101823.
- [43] D. Moreno Nieto, V. Casal López, S. I. Molina, *Addit. Manuf.* **2018**, *23*, 79.
- [44] International Organization for Standardization, Prosthetics — Structural Testing of Lower-Limb Prostheses — Requirements and Test Methods **2016**, (ISO Standard No. 10328:2016), <https://www.iso.org/standard/70205.html>.
- [45] PLA – Ultimaker Support, Available at: <https://support.ultimaker.com/hc/en-us/sections/360003504300>, (accessed: April 2022)